Journal of ELECTRONIC MATERIALS, Vol. 35, No. 7, 2006 *Regular Issue Paper*

Investigation of Electroless Cobalt-Phosphorous Layer and Its Diffusion Barrier Properties of Pb-Sn Solder

MUH-WANG LIANG,[1,2] HUI-TING YEN,[1] and TSUNG-EONG HSIEH[1]

1.—Department of Materials Science and Engineering, National Chiao Tung University, Hsinchu, Taiwan 30010, R.O.C. 2.—E-mail: MWLiang@itri.org.tw

The capability of a cobalt-phosphorous [Co(P)] layer, which was grown via the electroless plating process, to serve as the diffusion barrier of lead-tin (PbSn) solder was investigated in this work. The Auger electron spectroscopy (AES) and energy dispersive spectrometry (EDX) indicated that the phosphorous contents in Co(P) films decrease with increasing film thickness and that the average contents are no less than 8.7 at.% for the specimens prepared in this work. X-ray diffraction in conjunction with composition analyses revealed that the electroless Co(P) layer was a mixture of amorphous and nanocrystalline structures; however, the AES depth profile and subsequent analyses indicated that the first-formed Co(P) layer should be amorphous because it contains as much as 18 at.% P. This implied a good barrier capability for electroless Co(P) because, as revealed by EDX line scan, the Sn and Cu atoms could not penetrate the Co(P) layer after the PbSn/Cu/Co(P)/Cu/Ti/Si sample was subjected to annealing at 250°C in a forming gas ambient for 24 h. The fact that Sn and Cu underlayers could not penetrate the Co layer after such a liquid-state annealing step was evidence that the Co(P) layer may simultaneously serve as a diffusion-barrier interlayer dielectric and as an under-bump metallization for flip-chip copper (Cu) ICs.

Key words: Electroless plating, cobalt-phosphorous, diffusion barrier

INTRODUCTION

Under bump metallization (UBM) provides good adhesion between the bonding pads and the bumps and serves as a diffusion barrier, a wetting layer, and a protective layer for flip-chip bonding. There are mainly four types of diffusion barrier layer: sacrificial barriers, stuffed barriers, passive compound barriers, and amorphous barriers.[1] The most common materials used in UBM as diffusion-barrier layers are refractory metals, such as titanium (Ti), tungsten (W), molybdenum (Mo), and alloys thereof. All of these metals have superior diffusion-barrier capability at high temperatures and are in general deposited by physical vapor deposition (PVD). However, when PVD is used as in the recently described deep-submicron Cu-IC processes, the PVD suffers from poor step coverage.[2] Much effort has been expended to solve this difficulty, and one idea that has surfaced is that of the diffusion-barrier layer in the Cu-IC process being formed by an electroless plating method;[2,3] presently, the electroless plated nickel (Ni) is most commonly adopted for UBM.[4–7]

(Received October 28, 2005; accepted February 13, 2006)

Nickel has relatively low diffusion and reaction rates with solder, and a Ni layer 5 μm thick provides suitable reliability for UBM applications. Further, the low stress status of electroless Ni is more advantageous than that of Ni prepared by sputtering.[8] Because the plating baths for electroless Ni in general contain sodium hypophosphite (NaH_2PO_2) as the reducing agent, phosphorus (P) atoms are deposited simultaneously so that electroless Ni is in fact a nickel-phosphorous alloy [Ni(P)]. It is known that the phosphorous content in Ni(P) can be adjusted by the pH value of the plating bath and that the crystalline structure of Ni(P) changes with phosphorous content.[7,9] The mixture of microcrystalline and amorphous grains constitutes the Ni(P) when phosphorous content is in the range of 7–10 wt.%; when phosphorous content exceeds 10 wt.%, the Ni(P) layer becomes amorphous. The amorphous electroless Ni(P) possesses good barrier properties due to the nonexistence of fast diffusion paths, such as grain boundaries.

Electroless cobalt-phosphorous alloys [Co(P)] serving as diffusion barriers of Cu and polyimide dielectrics in multilayer microelectronic structures

have been studied by O'Sullivan et al.[10] Their investigation showed that electroless Co(P) is highly effective in inhibiting Cu diffusion at elevated temperatures, even at Co(P) thickness as low as 50 nm. The electroless Co(P) also exhibited a better diffusion-barrier effectiveness in comparison with Ni(P) and pure metals (Co, Ni). Study of electroless Co(P) further indicated that phosphorous co-deposition behaviors and its effects on the crystalline structure of Co(P) are similar to those of electroless Ni(P). Binary phase diagrams revealed relativity low solubility of Sn or Pb in Co;[11] it can thus be speculated that electroless Co(P) should possesses good barrier capabilities for UBM applications.

Studies have been made investigating the use of electroplated or PVD Co in UBM for the solder bump.[12,13] Because the Co layers prepared by these methods are polycrystalline, either W or P elements were doped into the Co layer to clog up the grain boundaries, thereby improving their ability to retard diffusion. For instance, the $Co_{0.9}W_{0.02}P_{0.08}$ alloy exhibited better barrier properties in comparison with $Co_{0.9}P_{0.1}$ and was capable of withstanding annealing at 450°C.[14,15] However, electroplating is not suitable for ceramic or organic substrates in the UBM process. PVD methods, such as sputtering, are costly. Electroless plating is a selective chemical deposition method; it can reduce the bumping cost significantly because it does not require masking or metal sputtering.[6] This technique easily allows parallel processing of multiple wafers so that it can offer high throughput. As the capability of electroless Co(P) as a barrier layer in UBM structure remains to be explored, we carried out this study in order to investigate its feasibility to serve both as the barrier layer in interlayer dielectrics and in UBM for flip-chip Cu-ICs.

EXPERIMENTAL PROCEDURES

Specimen Preparation

After the simulated Ti/Cu circuit layer on the Si substrate had been formed by e-beam evaporation and then processed by roughening/sensitization/activation, the specimens were subjected to electroless plating of different periods of times for depositing Co(P) layer. Table I lists the methods and solutions for roughening, sensitization, and activation. After the catalytic layer was formed on the specimens, a Co(P) layer was deposited thereon by means of the electroless plating solution defined in Table II, the pH of which was regulated by 3 M NaOH. In this experiment, plating conditions were as follows: pH value = 7.8 ± 0.3, temperature = 75 ± 2°C, V/A (mL/cm^2) ≥ 20, and plating time was adjustable with respect to the required thickness. A surface profiler (KLA-TENCOR P-10, California) measured the thickness of the Co(P) layer on substrates subjected to different plating times, and the plating rate was obtained. After the specimens were washed by DI water and then blown dry by a nitrogen jet, a Cu wetting layer of 800 nm and eutectic PbSn solder layer were sequentially deposited thereon. The PbSn/Cu/Co(P)/Cu/Ti/Si specimens were then annealed in a furnace at 250°C in an ambient of forming gas (5% H_2/95% N_2) for 0, 0.5, 6, 18, and 24 h, respectively. The procedure for specimen preparation is summarized in Fig. 1.

Table I. Solution for Roughening, Sensitization, Activation, and Immersion Time

Step	Composition	Concentration	Immersion Time
Roughening	H_2SO_4	5 wt.%	10 min
Sensitization	$SnCl_2{\cdot}2H_2O$	10 g/L	10 min
	HCL	40 mL/L	
Activation	$PdCl_2$	0.1 g/L	45 sec
	HCL	8 mL/L	

Table II. Compositions of Electroless Plating Bath

Composition	Concentration (g/L)
$CoSO_4{\cdot}7H_2O$	35
$NaH_2PO_2{\cdot}H_2O$	40
Na citrate	35
$(NH_4)_2SO_4$	70

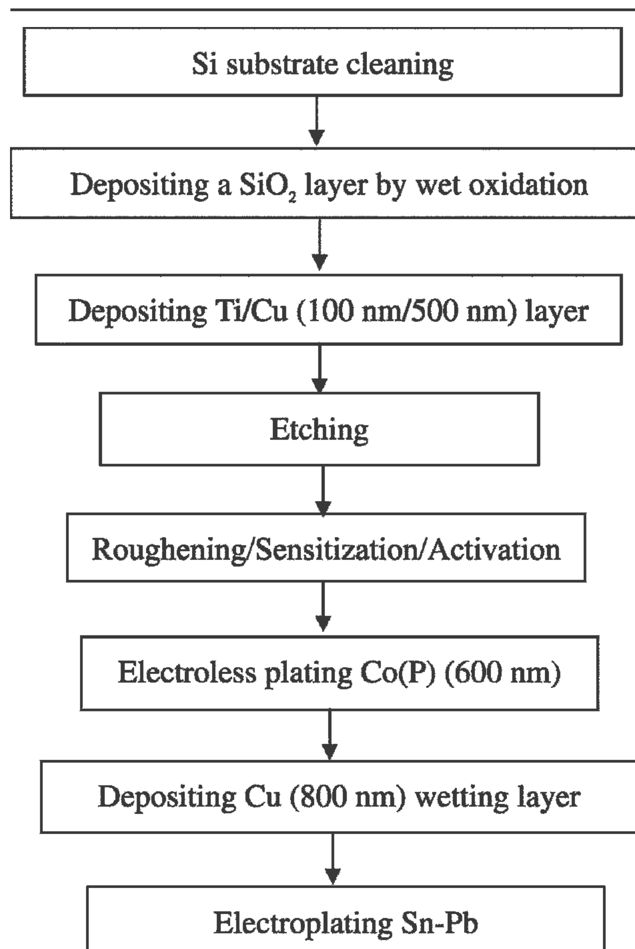

Fig. 1. Flowchart of specimen preparation.

Structure, Morphology, and Composition Characterization

The crystal structures of electroless Co(P) films were characterized by x-ray diffractometry (M18 XHF, MacScience). The x-ray source was Cu K_α radiation of wavelength 0.154 nm, operated at 200 mA and 50 kV, with a scan rate of 4°/min.

Scanning electron microscopy (SEM, FE-SEM JSM-6500F or FE-SEM Hitachi S-4700) was used to examine the morphology and cross-sectional structures of each specimen. Composition analysis was performed using Auger electron spectroscopy (AES, VG350) and energy dispersive spectrometry (EDX, Oxford Inca Energy 300) attached to the SEM. In addition, the EDX line scan was adopted to analyze the composition change for cross-sectional specimens subjected to different durations of thermal treatment. The line scan started from the Cu layer of the substrate and continued toward the PbSn solder, adopting at least four points of each specimen for analysis so as to obtain the averages thereof for further discussion.

RESULTS AND DISCUSSION

Deposition Rate of Electroless Co(P) Layer

Figure 2 is a profile showing plating time vs. thickness of electroless Co(P). At the beginning of the plating process, the deposition rate was faster because the concentration of the plating bath is higher; the thickness could reach 100 nm in the first 30 s, while the average plating rate is 130 nm/min. The chemical reaction formula of electroless plating Co(P) indicates that the deposition rate increase with the increase of pH value because an alkaline environment is preferred for electron release.[10] Table III shows average thicknesses of plated layers under conditions of different pH values at 75°C. Note that the thickness of the plated layer increases as the pH value increases, which reveals that the alkaline environment is beneficial for increasing the deposition rate. In addition, chemical reactions can be enhanced by increasing the temperature, such that the higher the temperature, the faster the deposition rate.

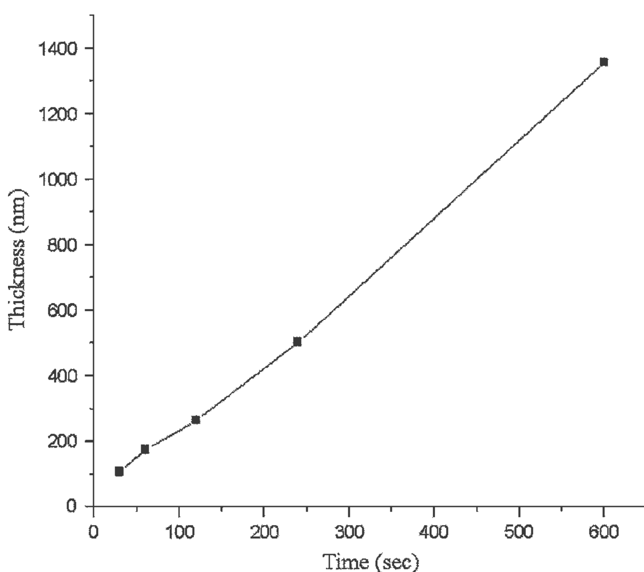

Fig. 2. Thickness of electroless plating Co(P) layer vs. deposition time.

Table III. Average Thickness of Plated Co(P) Layer

pH value	Average Thickness for 30 sec (nm)
7.5	100
8.0	160
8.5	250

Morphologies of Electroless Co(P) Layer

The number and size of palladium (Pd) granules formed on the sample were affected by the time that the sample was immersed in the activation solution. If the activation time was too short, the Pd granules were insufficient to cover the sample completely. If the activation time was too long, the size of each Pd grain might exceed 100 nm and too many Pd precipitates could be formed and left in the plating bath. It was found that an experimental activation time of ~45 sec could produce Pd granules of size 20–30 nm uniformly covering the substrate surface.

In addition to the phosphorous content of the plated layer, variation of pH values also affects the clustering of Co(P) nucleation. Figure 3 shows the morphologies of Co(P) layers deposited on the polished Cu plate after immersion in plating baths of different pH values for 60 sec each. Noted that the size of Co(P) clusters increases as the pH increases, whereas surface coverage is best at pH = 8.5. The structure of Co(P) clusters changes into conifer-leaf shape at pH = 9.0. Because the Co(P) layer was formed by replacing the activated Pd atoms, the density and the continuity of the electroless Co(P) layer were affected by the cluster condition of Pd atoms and the condition of the substrate surface. As revealed by subsequent SEM and XRD analyses, the many particles formed on the specimen surface were not caused by the crystallization during electroless plating, but rather by clustering effects. Clusters grew as deposition time increased, and eventually the clusters became large particles.

Composition Analysis of Electroless Co(P) Layer

It is known that the amount of phosphorous content in Co(P) film affects the structure and surface morphology of the plated films. When the phosphorous content in Co(P) film is within the range of 8–10 at.%, the formed crystal grain is nanocrystalline. When the phosphorous content in Co(P) film is within the range of 10–12 at.%, the electroless Co(P) layers are mixtures of amorphous and nanocrystalline structures. When the phosphorous content in Co(P)

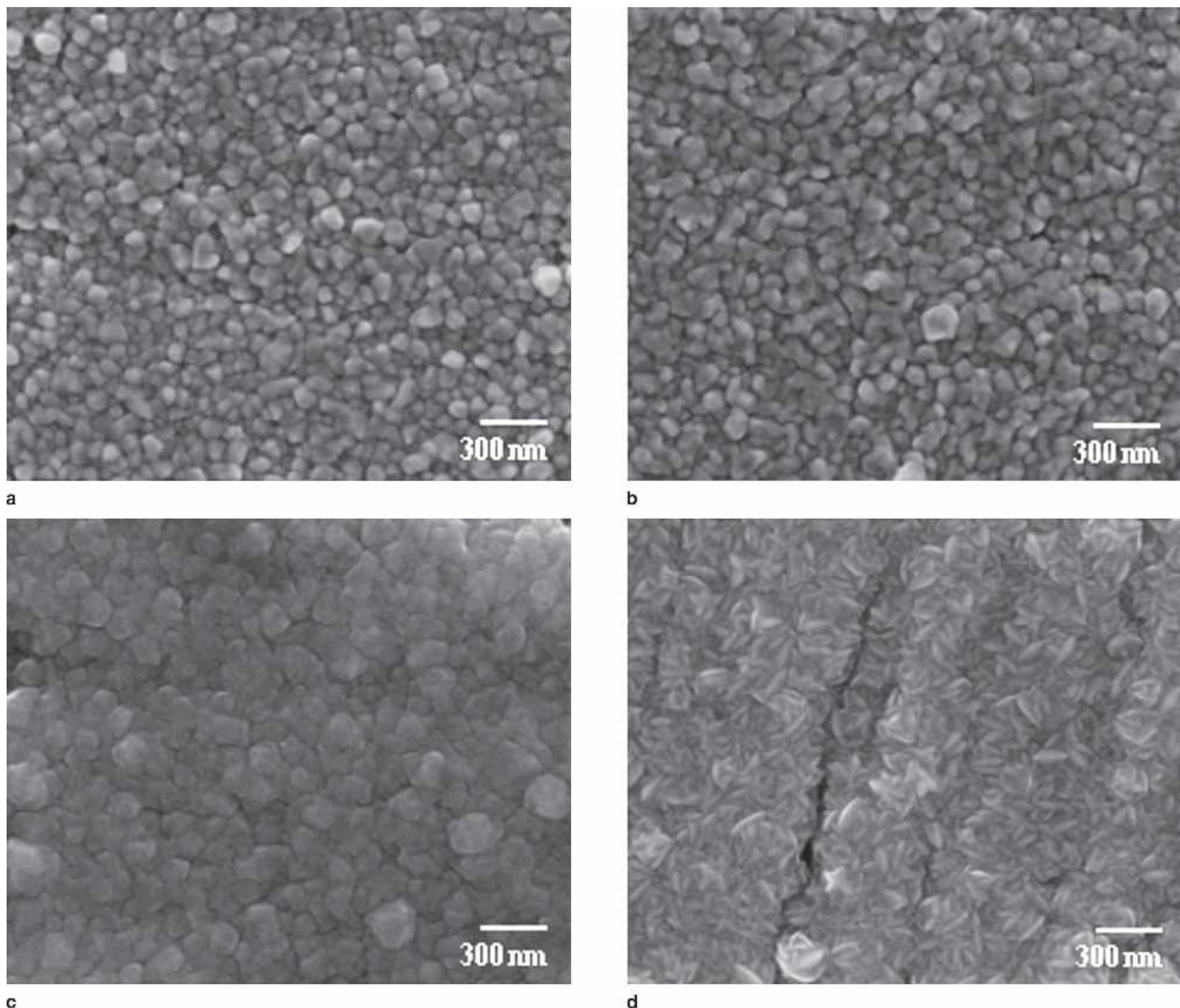

Fig. 3. Surface morphologies of Co layers deposited at different pH values: (a) 7.5; (b) 8.0; (c) 8.5; (d) 9.0.

film exceeds 12 at.%, the electroless Co(P) layers have an amorphous structure.[16] The amorphous structure starts to crystallize into α-Co at ~290°C, and orthorhombic crystals of Co_2P appear at 420°C.[15] Thermal treatment of the present experiment occurred at 250°C, so that the two types of Co crystals would not appear in the same experiment. According to composition analysis of the Co(P) thin film, the phosphorous content in the Co(P) film varied with changes in the deposition time. As seen in Table IV, the phosphorous content in the Co(P) film decreases as deposition time increases, but the minimum amount is still >8.7 at.% at any deposition time. Therefore, specimens of this experiment had nanocrystalline and amorphous structures, which was proven by subsequent XRD analysis.

Figure 4 shows an AES analysis depicting the depth profile of a 600-nm electroless Co(P) layer with 5-min. deposition time. The horizontal axis represents the depth of the Co(P) layer from the surface down, and the vertical axis represents the average phosphorous content of a 100-nm thick Co(P) film. As seen in Fig. 4, the phosphorous content increases with the depth of the Co(P) layer, and, at the interface between the Co(P) and the Ti/Cu layers, the phosphorous content reaches its maximum, i.e., ~18 at.%. To sum up, the phosphorous content is the highest at the beginning of the

Table IV. EDX Phosphorous Contents with Respect to Different Deposition Times

Deposition Time (sec)	Co (at.%)	P (at.%)
30	85.0	15.0
60	86.0	14.0
120	86.7	13.3
240	89.7	10.3
600	91.3	8.7

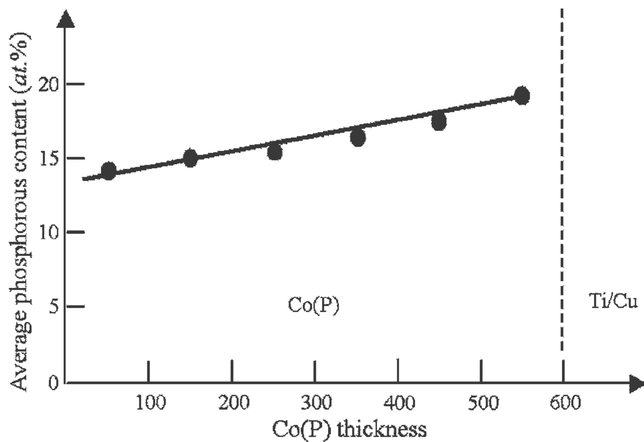

Fig. 4. Average phosphorous content of electroless Co(P) analyzed by AES.

electroless plating and decreases gradually as deposition time progresses. It was speculated that, with the increase of deposition time, the electroless Co(P) structure is in transition from amorphous to nanocrystalline or even polycrystalline structure.

XRD Analysis of the Plated Layer

As seen in Fig. 5, the 30-sec Co(P) layer has no obvious Co peak, but it does have has only two Cu (111) and (200) peaks; therefore, in conjunction with previous AES analysis, it can be concluded that, at the early stages of plating, the electroless Co(P) layer formed is amorphous. With increasing deposition time, the height of Co peaks increases while that of the Cu peaks decreases relatively. For a specimen being plated for 600 sec, the peak corresponding to $(01\bar{1}0)$ is significant compared to those corresponding to (0002) and $(01\bar{1}1)$. Therefore, the nanocrystalline structure grows as the phosphorus content decreases. With an increase in deposition time, the nanocrystalline area was gradually amplified, and thereby significant Co peaks were observed in the XRD pattern. Figure 6 shows the XRD pattern of Co(P) films deposited for 30 min., whose thickness is ~2.5 μm. As seen in Fig. 6, the pronounced Co peaks corresponding to $(01\bar{1}0)$, (0002), and $(01\bar{1}1)$ reveal that the 30-min. Co(P) film has a polycrystalline structure.

The grain sizes in the Co(P) film can be estimated by using Scherrer's formula[17] incorporating the XRD peak information:

$$t = \frac{0.9\lambda}{B\cos\theta},$$

where t corresponds to the grain size of crystal, λ is wavelength of the x-ray (0.154 nm), B represents the half-height width of the XRD peak, and θ represents the Bragg angle. The calculated grain sizes of the 60-s and 30-min. Co(P) layers were ~8.42 nm and ~34 nm, respectively. Moreover, the 600-s Co(P) layer formed a nanocrystalline structure with a grain size of 20–30 nm. According to the EDX analysis (Table IV), the phosphorous content of the 30-sec deposition film reaches 15.0 at.%. The phosphorous content decreases as the deposition time increases, and the structure of the Co(P) film varied, too. Because the concentration of $(HPO_2^-)_{ads}$ was at its maximum at the beginning of the electroless plating, the driving force for the reduction was also

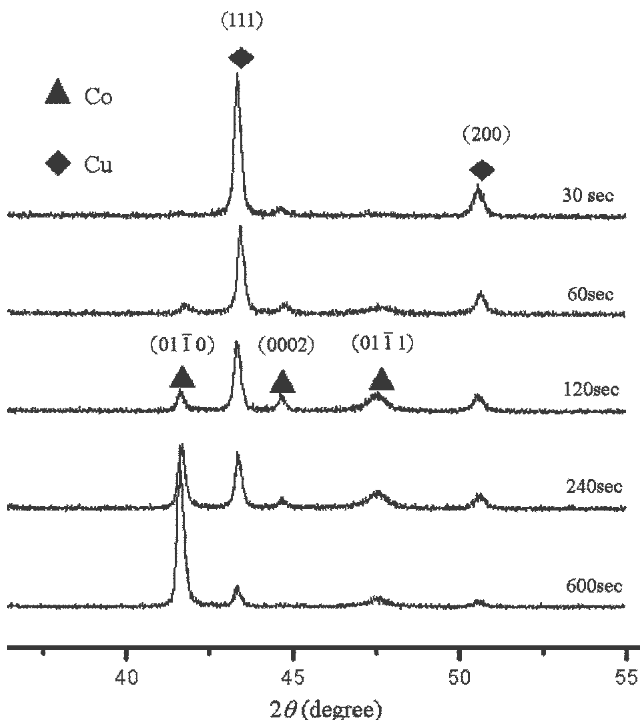

Fig. 5. XRD analysis performed on Co(P) films with different deposition times.

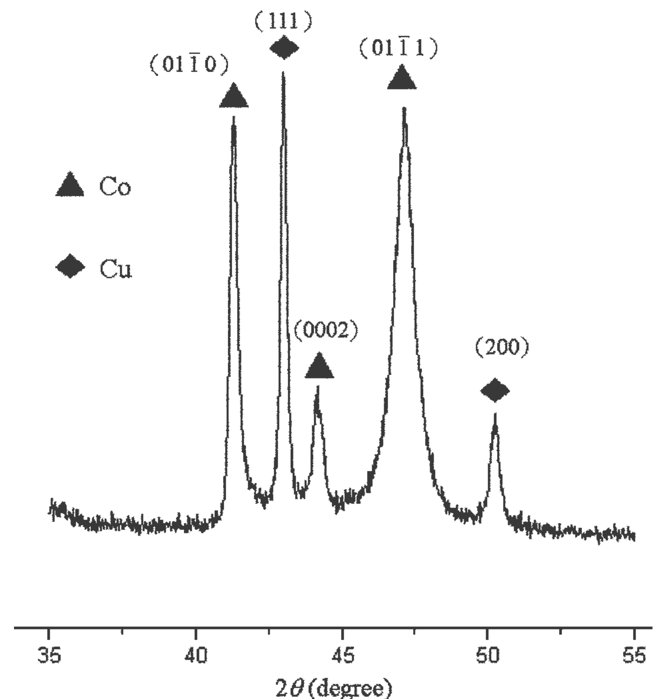

Fig. 6. XRD analysis performed on Co(P) films with 30-min. deposition time.

at its maximum and thus the amount of phosphorus being deposited was at its relative maximum.[10] Because the plating process is a chemical reaction rather than a physical change, the phosphorous content in the plated film changes during the chemical reaction. The fact that the phosphorous content in the plated film decreases with a decrease in the concentration of $(HPO_2^-)_{ads}$ hence causes the microstructural changes in the electroless plating film. It can thus be speculated that a Co(P) layer of amorphous structure formed at the beginning of the plating process can retard the diffusion of Sn and Cu atoms.

Interfacial Reactions of Electroless Co(P) Layer and Pb-Sn Solder

Because the specimens were treated at 250°C, which is higher than the eutectic temperature of Pb-Sn solder, the interfacial diffusion of present experiment progressed in the liquid state. The Cu wetting layer reacted with the Pb-Sn solder first, and the intermetallic compounds (IMCs) were produced. The IMCs produced under different durations of thermal treatment were subjected to EDX analysis, and the results are shown in Table V. Noted that the ratio of Cu and Sn falls in the range of 1.5–2.0, such that the IMCs could be a mixture of Cu_6Sn_5 and Cu_3Sn. This emergence of a Cu_3Sn phase could result from prolonged thermal treatment at a temperature relatively higher than the eutectic temperature of the Pb-Sn solder.

Figures 7a and b present the cross-sectional SEM micrographs and results of EDX line scan for the 6- and 24-h annealed specimens, respectively. In either case, the peak representing Sn abruptly decays when it reaches the Co(P) layer. This evidences that Sn could not penetrate the Co(P) layer after such a liquid-state annealing, and hence the Co(P) layer clearly serves as a good diffusion barrier for UBM structures. In the foregoing XRD analysis, it was speculated that the first-formed Co(P) layer is high in phosphorous content and thus should be amorphous. The fact that Sn could not penetrate the Co(P) layer revealed in the EDX line scan analysis further proves the speculation. Moreover, it is noted that peaks representing Co and Cu underlayers are separated without overlapping. Hence, Cu could not penetrate a Co(P) layer, either. Thus, the electroless Co(P) layer can serve as a good diffusion barrier of UBM structure for both Cu interconnects and solder bumping of flip-chip Cu-ICs.

Table V. EDX Analysis of IMCs Produced under Different Durations of Thermal Treatment

Thermal Duration (h)	Ratio (Cu/Sn)
0.5	2
6	1.65
18	1.73
24	1.56

CONCLUSIONS

This work studies the electroless plating of a Co(P) layer and its feasibility in UBM structures. At the beginning of the plating process, the deposition rate of Co(P) layer was at its fastest because the concentration of the plating bath was relatively high. The chemical reactions of electroless plating Co(P) indicated that the deposition rate increased with increasing pH values. AES and EDX analyses indicated that the phosphorous contents in Co(P)

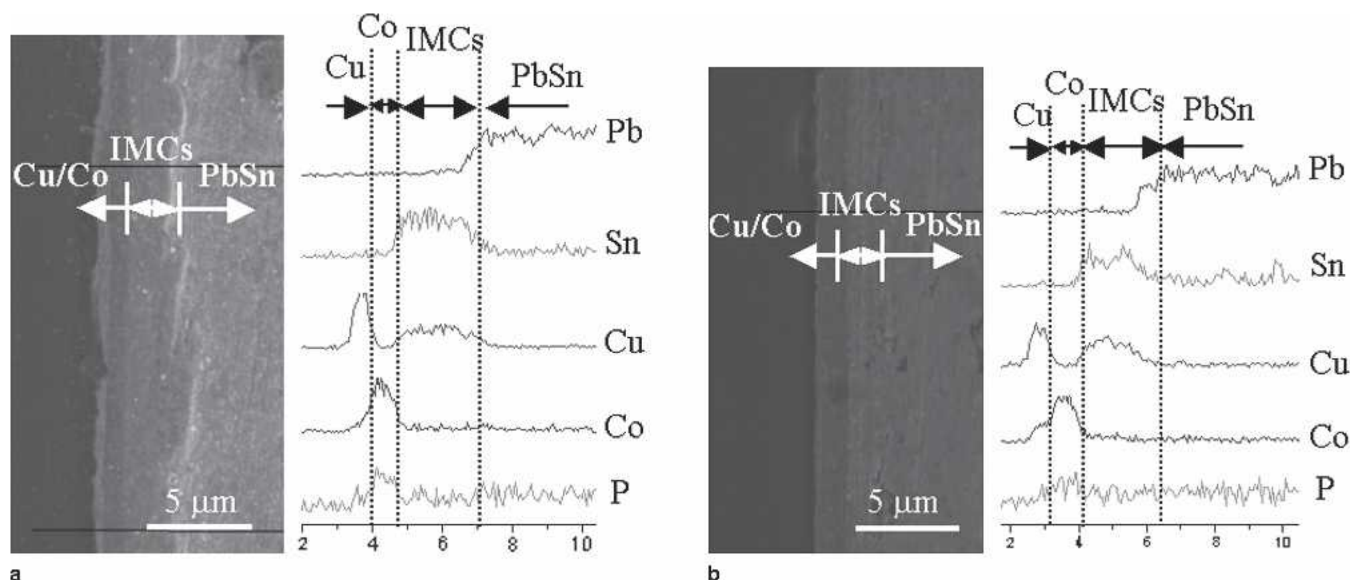

Fig. 7. Cross-sectional SEM view of specimen interfaces and corresponding line-scanning EDX analyses after annealing at 250°C for (a) 6 h and (b) 24 h.

films decreased with increases of film thickness and that average contents are no less than 8.7 at.% for the specimens. Although XRD in conjunction with composition analyses revealed that the electroless Co(P) layer prepared in this work was a mixture of amorphous and nanocrystalline structures, the AES depth profile analysis revealed that the phosphorous content in Co(P) film formed at the beginning of the plating process could reach a concentration as high as 18 at.%. This implied that the first-formed electroless Co(P) layer is amorphous, and that it would possess a good ability to retard diffusion. As revealed by the EDX line-scan analysis, neither Sn nor Cu underlayers could penetrate the electroless Co(P) layer in the PbSn/Cu/Co(P)/Cu/Ti/Si sample subjected to annealing at 250°C in a forming gas ambient for 24 h. The EDX analysis also indicated that, in addition to the formation of Cu_6Sn_5 and Cu_3Sn phases, diffusion of Co atoms into the solder region was negligible, and no metallurgical reaction could be observed. Hence the electroless Co(P) layer may simultaneously serve as a diffusion barrier of Cu interconnects and as an UBM structure in flip-chip Cu-ICs.

ACKNOWLEDGEMENTS

This work was supported by the Department of Industrial Technology, Ministry of Economics Affairs of the ROC under TDPA (Technology Development Program for Academia, Contract No. 92-EC-17-A-05-S1-020), and the National Science Council of the R.O.C. (Contract No. NSC93-2216-E-009-008).

REFERENCES

1. T.T. Kodas and M.J. Hampden-Smith, ed., *The Chemistry of Metal CVD* (New York: VCH, 1994), p. 9.
2. C.-Y. Lee, T.-H. Huang, and S.-C. Lu, *J. Mater. Sci.* 9, 337 (1998).
3. M. Paunovic, P.J. Bailey, and R.G. Schad, *J. Electrochem. Soc.* 141, 337 (1994).
4. J.H. Lau, *Flip Chip Technologies* (New York: McGraw-Hill, 1996).
5. T. Oppert, E. Zakel, and T. Teutsch, *Proc. IEMT/IMC Symp*. Tokyo, *Japan* (Piscataway, NJ: IEEE, 1998), p. 106.
6. T. Teutsch, T. Oppert, E. Zakel, and E. Klusmann, *Electronic Components and Technology Conference (ECTC)*, Las Vegas, NV (Piscataway, NJ: IEEE, 2000), p. 107.
7. G.O. Mallory and J.B. Hajdu, *Electroless Plating Fundamentals and Applications* (Orlando, FL: AESF, 1990), Chap. 1-7.
8. R.H. Uang, K.C. Chen, S.W. Lu, H.T. Hu, and S.H. Huang, *IEEE Electron. Packag. Technol. Conf*. Singapore (Piscataway, NJ: IEEE, 2000), p. 292.
9. G.G. Gawrilov, *Chemical (Electroless) Nickel-Plating* (Redhill: Portcullis Press, 1974), Chap. 5.
10. E.J. O'Sullivan, A.G. Schrott, M. Paunovic, C.J. Sambucetti, J.R. Marino, P.J. Bailey, S. Kaja, and K.W. Semkow, *IBM J. Res. Dev*. 42, 607 (1998).
11. B. Thaddeus, X. Massalski, J.L. Murray, L.H. Bennett, and H. Baker, *Binary Alloy Phase Diagrams* (Metals Park, OH: American Society for Metals, 1986).
12. R. Labie, E. Beyne, and P. Ratchev, *Electronic Components and Technology Conference* (*ETCT*), (Piscataway, NJ: IEEE, 2003), p. 1230.
13. R. Labie, E. Beyne, R. Mertens, P. Ratchev, and J. Van Humbeeck, *IEEE Electron. Packag. Technol. Conf.* Singapore (Piscataway, NJ: IEEE, 2003), p. 584.
14. A. Kohn, M. Eizenberg, and Y. Shacham-Diamand, *J. Appl. Phys.* 92, 5508 (2002).
15. A. Kohn, M. Eizenberg, and Y. Shacham-Diamand, *Appl. Surf. Sci.* 212, 367 (2003).
16. L.A. Chekanova, E.A. Denisova, and R.S. Iskhakov, *IEEE Trans. Magn.* 33, 3730 (1997).
17. B.D. Cullity and S.R. Stock, *Elements of X-Ray Diffraction*, 3rd ed. (New Jersey: Prentice Hall, 2001).